AD-A016 667

OPTICALLY PUMPED LASER

Robert T. Brown

United Technologies Research Center

Prepared for:

Office of Naval Research

15 October 1975

OPTICALLY PUMPED LASER

Annual Technical Report

October 15, 1975

For period covering
August 15, 1974 To August 15, 1975

Sponsored By

Advanced Research Projects Agency

ARPA Order No. 1807

Contract No. N00014-74-C-0376

R.T. Brown

The views and conclusions contained in this document are those of the author and should not be interpreted as necessarily representing the official policies, either expressed or implied, of the Advanced Research Projects Agency or the U.S. Government.

United Aircraft
Research Laboratories

UNITED AIRCRAFT CORPORATION

EAST HARTFORD, CONNECTICUT 06108

SECURITY CLASSIFICATION OF THIS PAGE (When Data Entered)

REPORT DOCUMENTATION PAGE		READ INSTRUCTIONS BEFORE COMPLETING FORM
1. REPORT NUMBER R75-921853-7	2. GOVT ACCESSION NO.	3. RECIPIENT'S CATALOG NUMBER
4. TITLE (and Subtitle) OPTICALLY PUMPED LASER		5. TYPE OF REPORT & PERIOD COVERED Annual Tech. 8/15/74 - 8/15/75 6. PERFORMING ORG. REPORT NUMBER R75-921853-7
7. AUTHOR(s) Robert T. Brown		8. CONTRACT OR GRANT NUMBER(s) N00014-74-C-0376
9. PERFORMING ORGANIZATION NAME AND ADDRESS United Technologies Research Center 400 Main Street East Hartford, CT 06108		10. PROGRAM ELEMENT, PROJECT, TASK AREA & WORK UNIT NUMBERS ARPA
11. CONTROLLING OFFICE NAME AND ADDRESS Office of Naval Research Department of Navy Arlington, VA 22217		12. REPORT DATE 10/15/75 13. NUMBER OF PAGES 47
14. MONITORING AGENCY NAME & ADDRESS(if different from Controlling Office) Director, Physics Programs Physical Sciences Division Office of Naval Research 800 North Quincy St., Arlington, VA 22217		15. SECURITY CLASS. (of this report) Unclassified 15a. DECLASSIFICATION/DOWNGRADING SCHEDULE

16. DISTRIBUTION STATEMENT (of this Report)

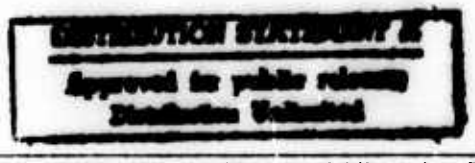

17. DISTRIBUTION STATEMENT (of the abstract entered in Block 20, if different from Report)

18. SUPPLEMENTARY NOTES

19. KEY WORDS (Continue on reverse side if necessary and identify by block number)

Optically-pumped electric-discharge laser
uv laser

20. ABSTRACT (Continue on reverse side if necessary and identify by block number)

This report describes experimental and theoretical studies of a new technique for pumping high-pressure electric-discharge lasers. Using a new Corporate-owned pumping laser, several significant results were achieved. A clear demonstration of lasing on the 3371 Å second positive transition in an optically-pumped electric discharge in a helium/nitrogen mixture was obtained. The peak uv signal was increased by three orders of

DD FORM 1 JAN 73 1473 EDITION OF 1 NOV 65 IS OBSOLETE

SECURITY CLASSIFICATION OF THIS PAGE (When Data Entered)

Block 20

magnitude over that obtained previously with the small TEA laser. Secondly, diffuse, high-electron-density, large-volume discharges were obtained in a geometry suitable for the incorporation of an optical cavity.

UNITED TECHNOLOGIES CORPORATION
RESEARCH CENTER

Report Number: R75-921853-7
Annual Technical Report for the period
15 August 1974 to 15 August 1975

OPTICALLY PUMPED LASER

ARPA Order No.:	1807
Program Code:	4E90K21
Contractor:	United Technologies Research Center
Effective Date of Contract:	1 March 1974
Contract Expiration Date:	15 October 1976
Amount of Contract:	$166,193*
Contract Number:	N00014-74-C-0376
Principal Investigator:	Dr. David C. Smith (203) 565-5281
Scientific Officer:	Director, Physics Programs Physical Sciences Division Office of Naval Research Department of the Navy 800 North Quincy Street Arlington, VA 22217
Short Title:	Optically Pumped Lasers
Report by:	R. T. Brown

*An ammendment to the contract increasing the amount to $285,043 has been signed by UTRC and returned to ARPA.

Sponsored By
Advanced Research Projects Agency
ARPA Order No. 1807

Optically Pumped Laser

TABLE OF CONTENTS

SECTION 1

ANNUAL TECHNICAL REPORT SUMMARY

Under this contract, a new technique for pumping high-pressure electric-discharge laser media is being investigated. The objective of this program is to develop high-energy, high-efficiency lasers operating in the ultraviolet and visible portions of the spectrum.

This report covers the period from August 15, 1974 to August 15, 1975. Preliminary work was carried out under an interim program, and was described in Ref. (Br 74). The basic elements of the optically-pumped electric discharge laser (OPEDL) concept can be explained in terms of the arrangement shown in Fig. 2.1. The output laser pulse from the TEA laser is focused into the active uv laser medium, which has been preionized to some low level of electron density. In the present studies, the preionization was produced via photoionization from small arcs in the uv laser medium. The 10.6 μ optical field then heats the electrons via inverse bremsstrahlung, and the electron density grows in a cascade process. The size of the discharge produced is determined by the size of the 10.6 μ laser focal volume and by the size of the region illuminated by the preionizing radiation. Since this discharge can have a very fast risetime and can reach very high electron densities, the discharge is well suited for pumping various uv and visible laser transitions.

During this reporting period a number of experiments were carried out using a Corporate-owned TEA laser with a nominal output of 15 J in a diffraction-limited beam. Based on these tests it was determined that a laser with more energy, better beam uniformity, and better pulse-to-pulse repeatability was required. A TEA laser with a nominal output of 75 J was purchased by United Technologies Corporation and was brought on line during the latter portion of the reporting period. With this system, the following significant results were achieved:

1. Clear demonstration of lasing on the 3371 Å 2nd positive transition in an optically-pumped electric discharge in a helium/nitrogen mixture. The peak uv signal was increased by three orders of magnitude over that obtained previously with the small TEA laser.

2. Generation of a diffuse, high-electron density discharge with dimensions 1 cm dia x 15 cm long in a helium-nitrogen mixture at 20 atmospheres. The gas mixture corresponded to a good operating point for the nitrogen ion-charge transfer laser, and the geometry was suitable for incorporating an optical cavity at 4278 Å into the cell.

Section 2 of this report is a brief description of the new TEA laser facility.

Section 3 is a detailed experimental and theoretical study of the OPEDL in a He/N_2 mixture. While this system has inherent efficiency limitations, it is a good system for making some of the laser tests, because of its very high gain, and provides a good check on the numerical modeling work, since the important kinetic rates are well known.

Section 4 is a similar study in the potentially more efficient $He/Ar/N_2$ excitation transfer system. Because of its lower gain, and because of a large uncertainty in some of the important rates, less progress has been made with this system.

Section 5 is a description of some of the very promising results obtained with a new pumping configuration.

SECTION 2

UPGRADED TEA LASER FACILITY

During the first half of the present reporting period, experiments were carried out using the TEA oscillator/amplifier system described in Ref. (Br 74). Because of variations in the transverse beam profile, and because of the rather large pulse-to-pulse variation in the output of the laser, this system was not suitable for some of the experiments of interest in the present program. During the latter portion of the reporting period, the Corporate-owned TEA laser facility was upgraded significantly with the purchase of a commercial TEA laser (Lumonics TEA 601 A). The properties of this laser are shown in Table 2.1. The transverse beam profile with multi-mode optics was examined by making burn patterns on wax-covered chart paper, and, from visual examination, appeared to be uniform to within ± 10% over an 8 cm x 8 cm cross section.

Because of the limited time available, only a small number of experiments with the new laser were carried out during this reporting period. However, as will be described later, several significant results were achieved which were not attainable with the old laser facility.

TABLE 2.1

Large CO_2 TEA Laser Characteristics

	Multi-mode Optics	Unstable Resonator Optics
Optical Energy/Pulse	75 Joules	50 Joules
% Energy in Peak	≈35%	≈50%
Peak Width	80 ns FWHM	≈80 ns FWHM
Max. Peak Power	≈300 MW	200-300 MW
Beam Divergence	3.5 mRad (θ/2)	0.5 mRad (θ/2)
Pulse Reproducibility	± 5% with 99%+ pulse reliability	
Beam Cross Section	≈9 x 10 cm	Annulus, 8.5 x 4.3 cm
Repetition Rate	6 PPM	

SECTION 3

STUDIES AT 3371 Å IN HELIUM/NITROGEN MIXTURES

3.1 Experimental Studies with the Small TEA Laser

The basic elements of the optically-pumped electric discharge concept, along with a description of some of the experimental apparatus was given in Ref. (Br74). During the present reporting period, experiments with the coaxial arrangement were extended to a wider range of conditions in order to provide a detailed comparison with the theoretical studies.

The experimental arrangement used in the present study was similar to that described in Ref. (Br74) with the exception that the test cell was re-designed to operate at pressures up to 20 atm. A diagram of the arrangement is shown in Fig. 3.1. The TEA laser was operated in an oscillator/amplifier configuration and produced pulses with 50 MW peak power, 0.5 mrad divergence, and a pulse shape having a 100 nsec wide leading spike followed by a 1.5 μsec tail. The laser tended to be self mode-locked, i.e., the pulse consisted of a series of short spikes within the gain-switched pulse envelope.

One of the objectives of these experiments was to study the ionization kinetics over a range of pressures and to determine whether diffuse discharges could be obtained at high pressures. Photographs of typical discharges, taken during the previous reporting period and reported in Ref. (Br74) are shown in Fig. 3.2. Figures 3.2-a and 3.2-b were obtained at a pressure p of 7.1 atm and correspond to nitrogen fractions X_{N2} just below and just above the breakdown threshold (the condition in which the 10.6 μ absorption length becomes short compared to the length of the laser focal volume). A similar effect is seen in Figs. 3.2-c and 3.2-d, obtained at 12.0 atm. In Fig. 3.2-d, the nitrogen fraction was held constant and the peak 10.6 μ intensity I_o was increased slightly. The focal volume in these experiments had a measured half-power diameter of 1.1 mm and a length of approximately 10 cm. The bright spots in Fig. 3.2-b and 3.2-d were the result of the diffuse discharge being overdriven, rather than the result of aerosol-induced breakdown, as occurs in laboratory air (SB75). Comparison of the properties in Figs. 3.2-a through 3.2-d along with the 10.6 μ absorption measurements in Ref. (BS73) indicated that the electron densities in Figs. 3.2-a and 3.2-c were in the 10^{15}-10^{17} cm^{-3} range.

A second objective of the experiments with the small CO_2 TEA laser was to obtain quantitative data demonstrating laser action on the $C(^3\pi_u)_{v'=0} \rightarrow B(^3\pi_g)_{v'=0}$ transition (3371 Å) in an optically-pumped He/N_2 discharge. In this series of experiments, attempts to incorporate a uv optical cavity into the pumping arrangement were not successful because of the need to isolate the 10.6 μ radiation from the uv radiation and the need to keep these isolating elements well away from the 10.6 μ focus. However, a large number of data were obtained which showed lasing via amplified-spontaneous-emission (Wa73).

As described in Ref. (Br74), a photodetector with a narrow-band filter at 3371 Å was used to monitor the radiation emitted along the axis of the discharge. Typical traces are shown in Fig. 3.3. Figure 3.3-a was taken with a very low nitrogen fraction and represents the spontaneous emission from the diffuse discharge. The spontaneous emission pulse had approximately the same shape as the TEA laser pumping pulse. Figures 3.3-b through 3.3-d represent increasing values of X_{N_2} with correspondingly increased values of I_o and show the development of an amplified-spontaneous-emission-spike (note scale changes) with increased nitrogen inversion densities. In Fig. 3.4 the experimental points were obtained at a fixed pressure and nitrogen fraction, but with increasing values of I_o and show an exponential increase with pumping intensity, characteristic of amplified-spontaneous-emission. The 3371 Å pulse shape and variation with I_o will be discussed in Section 3.3 below. The data in Figs. 3.3 and 3.4 clearly show the presence of laser action via amplified-spontaneous-emission. Because of the rather small size of the active discharge, the 3371 Å transition did not reach a saturated lasing condition in these experiments.

3.2 Theoretical Model

In order to gain insight into the kinetics of the optically-pumped He/N_2 discharge, and to aid in interpreting the experimental data, a numerical simulation of the kinetic processes has been developed. This model is similar to that described in References (Ge65) and (AKA67) for a conventional nitrogen laser. In the present model, processes involving quenching of the $C^3\pi_u$ and $B^3\pi_g$ levels by neutral molecules have been included since these processes can be important at the high pressures of interest with the optically-pumped discharge approach. The model assumes some initial value of electron density, and calculates the various discharge properties for a given 10.6 μ pulse shape and peak intensity. The processes considered in the model are listed in Table 3.1 and the governing rate equations can be written as follows.

Ionization rate equation:

$$\frac{d[e]}{dt} = [e]\, k_7\, [N_2{}^X] \,, \tag{3.1}$$

where $[e]$ is the electron density, $[N_2{}^X]$ is the nitrogen ground state density, and k_7 is the rate coefficient associated with process (7) in Table 3.1. Since we are interested in short time scales ($\leq$ 100 nsec), no loss processes have been included in the ionization rate equation. Also, for the range of electron energies and nitrogen fractions of interest here, the nitrogen dominates all of the inelastic processes. For the cases considered, process (8) was found to be negligible compared to process (7).

Excitation rate equations:

$$\frac{d\,[N_2{}^{C,O}]}{dt} = [e]\, k_5\, [N_2{}^X] - \frac{[N_2{}^{C,O}]}{\tau_C} - P \,,$$

$$\frac{d\,[N_2{}^{B,O}]}{dt} = [e]\, k_4\, [N_2{}^X] + \frac{[N_2{}^{C,O}]}{\tau_C} + P - \frac{[N_2{}^{B,O}]}{\tau_B} \,, \tag{3.2}$$

where

$$\tau_C = \left\{ k_{12} + [N_2{}^X]\, k_{14} + [He]\, k_{15} + [e]\, k_{16} \right\}^{-1}$$

$$\tau_B = \left\{ k_{13} + [N_2{}^X]\, k_{17} + [He]\, k_{18} \right\}^{-1} \,. \tag{3.3}$$

In these expressions, $[N_2{}^{C,O}]$ is the number density in the $C(^3\pi_u)_{v'=0}$ state of nitrogen, $[N_2{}^{B,O}]$ is the density in the $B(^3\pi_g)_{v'=0}$ state, P is the uv power density in photons/cm^3-sec, and the rates k_j refer to the processes in Table 3.1. For the conditions of interest here, process (6) was negligible compared to process (5).

Electron energy equation:

$$\frac{e^2\, I\, \nu}{m_e\, \varepsilon_o\, c\, (\omega^2 + \nu^2)} = \left\{ k_1\, \varepsilon_1 + k_2\, \varepsilon_2 + k_3\, \varepsilon_3 + k_7\, \varepsilon_7 + k_9\, \varepsilon_9 \right\} [N_2{}^X]$$
$$+ [N_2{}^X]\, k_{10}\, \frac{3}{2}\, \frac{m_e}{m_{N_2}}\, (\bar{u}_e - \bar{u}_g) + [He]\, k_{11}\, \frac{3}{2}\, \frac{m_e}{m_{He}}\, (\bar{u}_e - \bar{u}_g) \,, \tag{3.4}$$

where e is the electronic charge, I is the 10.6 μ intensity, ν is the momentum transfer collision frequency, m_e is the electron mass, ϵ_o is the free-space permittivity, c is the speed of light, ω is the laser angular frequency, $\bar{u}_e$ and $\bar{u}_g$ are the electron and gas temperatures, and the rates k_j and corresponding energies ϵ_j refer to Table 3.1. In the electron energy equation, the rates of electronic excitation to all vibrational levels are included since they represent electronic energy losses, even though only excitations to the ground vibrational levels are of importance in determining the population inversion.

In addition to the above equations, the vibrational temperature $\bar{u}_v$ and gas temperature $\bar{u}_g \equiv 3/2\ kT_g$ were calculated from the appropriate equations. These quantities were used primarily to check for depletion of the ground level due to electron excitation or to thermal excitation.

The various processes, along with the sources of the various rate data are shown in Table 3.1. The electron impact rates are plotted in Figure 3.5. These rates were obtained by integrating the appropriate cross sections over a maxwellian energy distribution function. The Cartwright cross section (Ca70) for the $X^1\Sigma_g^+ \rightarrow A^3\Sigma_u^+$ process was multiplied by the factor 1/3, based on the discussion in Ref. (Ca70) and in order to bring the value into better agreement with the value presented in Ref. (FPR64). For the same reasons, the cross section for the $X^1\Sigma_g^+ \rightarrow C^3\pi_u$ process was multiplied by the factor 1/1.5.

In addition to the above rate equations, the 10.6 μ absorption length ℓ_a was calculated from the expression

$$\ell_a = \frac{m_e\ \varepsilon_o\ c\ (\omega^2 + \nu^2)}{[e]\ e^2\ \nu} \quad . \tag{3.5}$$

3.3 Comparison of Theory with Experiment

As mentioned in Section 3.1, the experimental data were obtained under conditions in which the uv laser transition was not saturated. In order to compare the theoretical model with these data, calculations were carried out as follows. The uv power density P in Eqs. 3.2 and 3.3 was set equal to zero, giving three equations for the unknowns [e], $[N_2{}^C,{}^0]$ and $[N_2{}^B,{}^0]$, with Eq. 3.4 giving $\bar{u}_e$ for each value of I. Typical results are shown in Fig. 3.6, in which a 10.6 μ pulse shape approximating that in the experiments has been used, and where an initial electron density of 10^{11} cm^{-3} was assumed. The plots show the electron density and the inversion density vs time during the pumping pulse.

It should be pointed out that in the calculation, the 10.6 μ intensity was assumed to be uniform over the volume under consideration; wheras, in the experiment, the 10.6 μ intensity varied spatially due to the transverse beam profile, and due to the attenuation by the discharge. Thus, the calculation represents points near the centerline of the focal volume and is strictly valid only for conditions in which the absorption length ℓ_a is comparable to or greater than the focal volume length. For all of the curves in Fig. 3.6 the calculated absorption length was in excess of 50 cm (i.e. long compared to the 10 cm focal volume length) during the time in which an inversion existed.

Two trends are apparent from the curves in Fig. 3.6. First, the peak inversion occurred near the peak of the 10.6 μ pulse, and the inversion had a time duration of approximately 10 nsec, as would a pulse of amplified-spontaneous-emission radiation corresponding to this inversion. This trend is in qualitative agreement with the detector traces in Fig. 3.3. For these conditions, the decay time τ_C had a value of approximately 3 nsec, and as seen from Fig. 3.6 once the 10.6 μ intensity (and the electron temperature) began to fall, the inversion decayed on this same time scale.

A second trend seen in Fig. 3.6 is the strong dependence of the peak inversion density and of the electron density on the 10.6 μ intensity. While the experimental variation of electron density with I_o was not quite as rapid as indicated in Fig. 3.6, the dependence on I_o was still strong, as indicated in Figs. 3.2-c and 3.2-d. This effect required a high level of pulse-to-pulse repeatability in the TEA pumping laser in order to obtain reliable results with optical discharge pumping. In Fig. 3.4 the peak inversion densities, obtained from Fig. 3.6, are plotted for comparison with the peak uv signals. The inversion density (rather than the exponential of the inversion density) is probably a good comparison, since in the experiments the intense portion of the discharge (i.e., the effective gain length) appeared to decrease as the pumping intensity was increased. It can be seen that the two curves in Fig. 3.4 do show reasonably good agreement.

3.4 Coupling and Efficiency Calculations

In any practical laser utilizing the optically-pumped discharge concept, conditions would be chosen such that the uv radiation field would saturate the $C^3\pi_u \rightarrow B^3\pi_g$ transition (either through use of a uv optical cavity or by making the system large enough so that the amplified-spontaneous-emission intensity reached saturation (Le65)). This section describes results obtained modeling the latter condition. As discussed in Refs. (Ge65) and (AKA67), when the transition is saturated ($[N_2{}^{C,O}] \approx [N_2{}^{B,O}]$), Eqs. 3.2 can be re-written as

$$\frac{d\,[N_2^{C,O}]}{dt} = \frac{1}{2}\left\{[e]\,[N_2^{X}]\,[k_4 + k_5]\right\} - \frac{[N_2^{C,O}]}{2\,\tau_B}\,, \qquad (3.6)$$

and

$$P = \frac{1}{2}\left\{[e]\,[N_2^{X}]\,[k_5 - k_4] - \frac{2 - (\tau_C/\tau_B)}{\tau_C}\,[N_2^{C,O}]\right\}. \qquad (3.7)$$

In modeling large scale laser systems, the uv flux was treated in two ways. During the initial buildup of the electron density, the transition was assumed to be unsaturated, and the inversion was calculated using Eqs. 3.2 and 3.3 with P = 0. When the total gain reached 30 dB (using a cross section for stimulated emission of 10^{-15} cm^2), the transition was assumed to be saturated and the uv power was calculated using Eq. 3.7. This approach was qualitatively useful in determining the onset of lasing, and should give accurate quantitative results for conditions well above threshold.

The purpose of the saturated-power calculation was to investigate the energy transfer processes in the discharge and to examine the parameters which determine the efficiency of conversion from 10.6 μ radiation to 3371 Å radiation. In doing this, it was useful to define two efficiency factors. The coupling efficiency η_C can be defined as

$$\eta_C \equiv \frac{\text{power coupled into uv field}}{\text{power absorbed from 10.6}\mu\text{ field}}\,,$$

and can be written

$$\eta_C = \frac{P\varepsilon_\phi}{I_{10.6}/\ell_a}\,, \qquad (3.8)$$

where ε_ϕ is the photon energy. A total efficiency η_T can be defined as

$$\eta_T = \frac{\text{uv energy coupled out of the discharge}}{10.6\mu \text{ energy incident on the discharge}} ,$$

and can be written

$$\eta_T = \frac{\ell_d \int_o^T P\, \epsilon_\phi \, dt}{\int_o^T I \, dt} , \qquad (3.9)$$

where ℓ_d is the discharge length, and T is the 10.6 μ pulse length. (In this expression, it is assumed that the 10.6 μ focal volume and the uv laser axis are coaxial).

The quantity η_C can be interpreted as a microscopic efficiency and is a measure of the effectiveness with which the energy deposited in the electrons is converted into uv photons. The coupling efficiency can in turn be written as the product of three factors as

$$\eta_C = \eta_{EC}\, \eta_{CB}\, \eta_Q ,$$

where η_{EC} is the fraction of energy deposited in the electrons which channels into the upper laser level, η_{CB} is the fraction of energy in the upper level which goes into stimulated emission, rather than into spontaneous emission or quenching, and η_Q is the quantum efficiency ($\eta_Q = \epsilon_\phi/\epsilon_5$).

The factor η_{EC} can be examined directly by looking at Eq. 3.4. For most cases of interest, the elastic losses are negligible compared to the inelastic losses, and η_{EC} can be written

$$\eta_{EC} = \frac{k_5 \epsilon_5}{\sum_j k_j \epsilon_j} ,$$

where the summation is over the inelastic terms on the right hand side of Eq. 3.4. This quantity, which is a function only of the electron temperature, is plotted in Fig. 3.7. It can be seen that in order to keep this factor high, it is necessary to maintain $\bar{u}_e$ above 4 eV. A similar result was obtained in Ref. (AKA67).

The factor η_{CB} can be examined by looking at Eq. 3.7. The factor of one half can be interpreted physically as follows. Since the transition is bottlenecked ($\tau_C << \tau_B$) the inversion can only be maintained on a transient basis and each stimulated emission event reduces the inversion by two molecules. Thus, even under conditions where stimulated emission dominates spontaneous emission and quenching, the factor η_{CB} is limited to a value of 1/2.

Based on these arguments, the upper limit on the value of η_C for the 3371 Å nitrogen transition ($\eta_Q = 0.33$) is $\eta_C)_{max} \approx (0.10)\ (0.5)\ (0.33) = 0.016 = 1.6\%$. This result depends only on the collisional rates, and is independent of the method of electron heating (i.e., dc discharge, rf discharge, electron beam, or optically pumped discharge).

In developing a working laser, one cannot maintain η_C at its optimum value during the entire pumping pulse because of temporal and spatial variations in η_{EC} (through variations in $\bar{u}_e$) and in η_{CB} (due to such things as quenching and laser threshold effects). Thus, once one has selected a kinetic system with a reasonably high value of $\eta_C)_{max}$, the problem of optimizing the laser design becomes one of developing a pumping scheme which can maintain this value of η_C over the entire active volume and during a significant fraction of the pumping pulse.

This problem is very difficult in the nitrogen system because of the coupling between the laser kinetics and the ionization kinetics. As mentioned above, it is desirable to maintain $\bar{u}_e$ above the 4 eV. However, as seen from Fig. 3.5, for a nitrogen pressure of 50 torr, and $\bar{u}_e = 4$ eV, the ionization time $\tau_I = \{[N_2^X]k_7\}^{-1}$ is 0.5 nsec. Thus, the electron density builds up very quickly under optimum laser pumping conditions. In the dc discharge this results in a mismatch between the discharge impedance and the driving circuit with a corresponding drop in $\bar{u}_e$ and with a large fraction of the stored electrical energy being dissipated in the external circuit rather than in the discharge.

In the case of the optically-pumped discharge, the value of $\bar{u}_e$ can be maintained at a high value even for large values of [e] (see Eq. 3.4). However, if $\bar{u}_e$ is maintained at a high value for too long a period of time, the ionization process will go all the way to breakdown (See Fig. 3.2). Thus for both dc and optical pumping, the ionization process favors short pumping pulses, and tends to be an even more stringent constraint on the pulse width than laser bottlenecking, Ref. (Ge65).

Typical numerical results, illustrating some of these effects are shown in Figs. 3.8 and 3.9. In Fig. 3.8, a 10.6 μ pulse shape typical of that in the experiments was used. The onset of uv saturation was based on an active length of 100 cm, and the peak value of I was chosen so that ℓ_a

stayed above a value of 75 cm during the pulse. With these constraints, the coupling efficiency varied from ~0.8 percent at the beginning of the uv pulse to ~0.5 percent at the peak of the uv pulse. The corresponding total efficiency reached a peak value of 0.01 percent. The rapid cutoff of the uv pulse was caused by electron quenching.

The case shown in Fig. 3.9 represents a better match between the pumping pulse and the discharge kinetics. The nitrogen and helium densities were chosen so that their quenching rates were equal to the spontaneous emission rate from the $C^3\pi_u$ level. The 10.6 μ peak intensity and pulse shape were chosen so that $\bar{u}_e$ remained high during the uv pulse, but so that [e] remained low enough to reduce quenching of the $C^3\pi_u$ level. These conditions corresponded to $\ell_a)_{min}$ = 230 cm and a value ℓ_d = 500 cm was used. This result shows that for this kinetic system, the optical pumping approach becomes more favorable for very large laser systems.

The value of $\bar{u}_e$ for these conditions was higher than in Fig. 3.8, and η_C varied from 1.2 percent at the beginning of the uv pulse to 0.9 percent at the peak of the pulse. The corresponding total efficiency was 0.35 percent. The gas temperature reached a value of 307°K, and the vibrational temperature was 700°K at the end of the uv pulse, indicating that vibrational depopulation of the ground state would not be a problem. The results in Fig. 3.9 show that the electron temperature follows the 10.6 μ intensity directly, and that the coupling efficiency follows $\bar{u}_e$ during the time when the uv laser transition is saturated. The factor of 30 improvement in η_T from Fig. 3.8 to Fig. 3.9 resulted from the higher electron temperature during the uv pulse, from the better overlap between the uv pulse and the 10.6 μ pulse, and from the reduction of electron quenching of the upper laser level.

While Fig. 3.9 probably does not represent the optimum conditions, it does illustrate the approach that can be used in seeking the optimum set of parameters (e.g., pressure, nitrogen fraction, 10.6 μ pulse shape, 10.6 μ pulse length, discharge length, etc.). The peak value of η_C in Fig. 3.9 is close to the maximum value estimated above from simple energy channeling considerations and the total efficiency of 0.35 percent is within a factor of 4 of the maximum coupling efficiency. With further optimization, a total efficiency of 1 percent could probably be achieved. Since TEA lasers operating with pulses of the approximate shape shown in Fig. 3.9 could be expected to have an efficiency of 10%, the total efficiency of this system (stored electrical energy to uv laser energy) is probably limited to a value of 0.1 - 0.2 percent. While this value is comparable to values attainable with conventional large-volume nitrogen lasers (HPKB74), it is somewhat marginal for most large scale uv laser applications. For this reason, the optically-pumped discharge approach is probably of greater interest when applied to other kinetic systems (KFRE72, AB074, CCS74).

3.5 Experimental Studies with the Large TEA Laser

As mentioned in Section 2, a large CO_2 TEA laser was brought into operation during the latter part of the reporting period. The studies in helium/nitrogen mixtures were continued using the experimental arrangement shown in Fig. 3.10. The TEA laser was operated in an unstable resonator mode, giving properties nominally equal to those in Table 2.1. The 10.6 μ intensity at the focus of the 4.5 m focal-length mirror was varied by clipping the outer portion of the beam. Typical beam profiles are shown in Fig. 3.11. Typical photographs of the optically pumped discharge in a mixture of 5 percent nitrogen/95 percent helium are shown in Fig. 3.12, with the 10.6 μ peak intensity just below the breakdown threshold and just above the breakdown threshold. The beam profiles used were those in Fig. 3.11, and as seen from Fig. 3.11, only 10-20 percent of the output from the TEA laser was utilized to drive the discharged. The discharge in Fig. 3.12-a was ~ 0.5 cm in diameter by 42 cm in length.

When a piece of exposed-developed polaroid film was placed ~ 1 m from the quartz cell window, the pattern shown in Fig. 3.13 was obtained. It should be noted that there were no apertures in the cell, and the exit window aperture was 3.8 cm in diameter. Thus, the well defined spot size of ~ 2 cm diameter was an inherent property of the emitted radiation. The uv radiation was detected using the arrangement shown in Fig. 3.10 and had a pulse shape as shown in Fig. 3.13. The vertical scale is in the same relative units as in Fig. 3.3 and shows that the peak uv power was over 10^3 higher than in the experiments with the small TEA laser. (An approximate calibration of the uv detector system indicated a peak uv power of 200 W). The spiking in the uv pulse is evidently due to spiking in the CO_2 TEA laser. Spectral measurements of the radiation will be made in the near future. Preliminary spectral measurements, using various narrow-band filters, indicated that all of the radiation occurred at 3371 Å.

A second series of tests were made with a small aluminized mirror mounted just inside the Ge window on the cell. The mirror was ~ 1 cm in diameter, with a 4.0 m radius of curvature and was mounted on a thin spider. With this mirror properly aligned, a portion of the amplified-spontaneous-emission pulse emanating toward the TEA laser was reflected back through the discharge; in effect, operating as a single pass optical cavity. Figure 3.14 shows the fluorescence spots corresponding to two different conditions. In Fig. 3.14-a the uv mirror was intentionally misaligned to show the spot from the direct pulse (i.e., the same spot as in Fig. 3.13) and the spot from the reflected pulse. Figures 3.14-b and 3.14-c show the spot obtained with the uv mirror aligned, and clearly show the effect of laser amplification. The size of the amplified spot is comparable to the diameter of the optically-pumped discharge, as would be expected.

The uv mirror was approximately 1.8 m from the center of the discharge, giving rise to a 12 nsec delay in the amplified pulse relative to the direct pulse. Detector traces made with the single-pass cavity are shown in Fig. 3.15. Because of the random nature of the spiking from the TEA laser, there was considerable pulse-to-pulse variation in the uv pulse shape. However, it did appear that with the uv mirror aligned, an amplified pulse of approximately 12 nsec delay was detected.

These results indicate that the amplified-spontaneous-emission field was not saturating the medium, and that the uv energy output could be increased considerably by either making the discharge longer, or by incorporating a multipass cavity into the cell. Both of these approaches will be pursued during the next reporting period.

Table 3.1 (Cont'd)

Notes:

1. Cross section from Ref. (Ca 70) multiplied by 1/3 based on discussion in Ref. (Ca 70) and in order to bring the value into closer agreement with that in Ref. (EPR64).

2. Cross section from Ref. (Ca 70).

3. Cross section from Ref. (Ca 70) multiplied by 1/1.5 based on same arguments as note 1.

4. Cross section obtained from multiple-vibrational-level cross section by multiplying by appropriate Frank-Condon factor.

5. Rate from Ref. (AKA67).

6. Cross section from Ref. (Mc 64).

7. Rate from Ref. (HGHML74).

8. Rate estimated based on Ref. (HGHML74).

FIG. 3.1

EXPERIMENTAL ARRANGEMENT USING SMALL TEA LASER

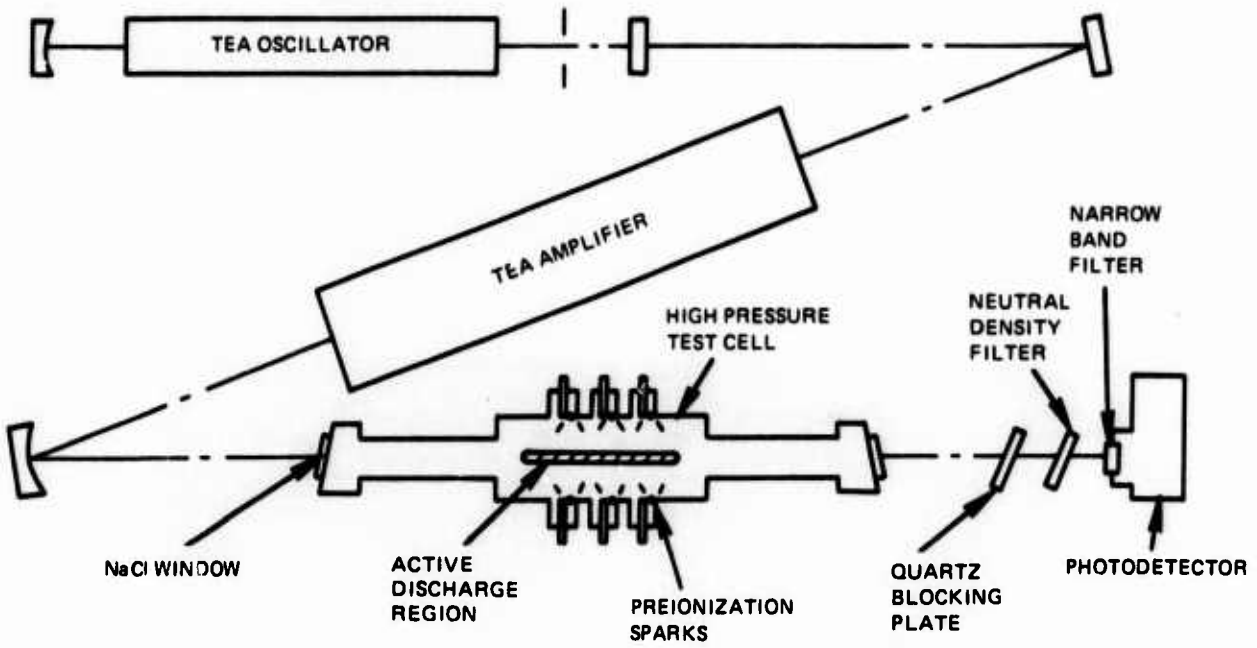

R09-194-1

OPTICALLY–PUMPED DISCHARGES IN HELIUM–NITROGEN MIXTURES

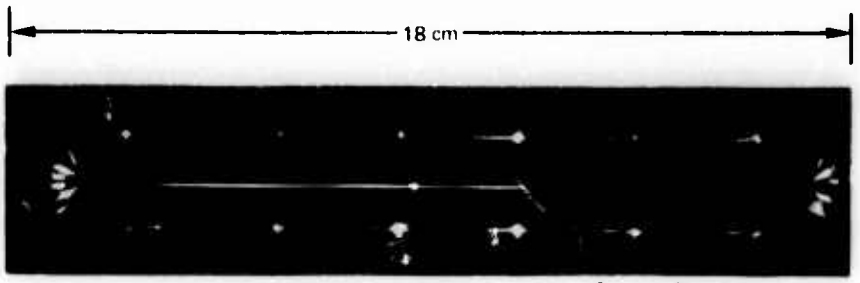

(a) p = 7.1 atm, X_{N_2} = 0.14, I_o = 1.6x10^9 W/cm^2

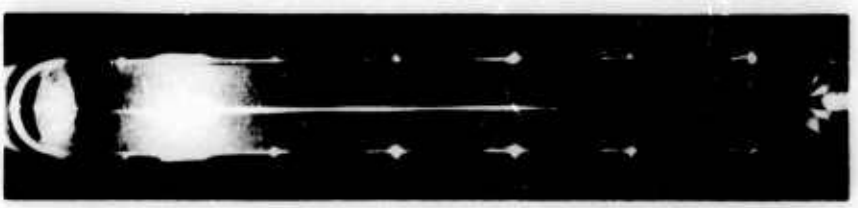

(b) p = 7.1 atm, X_{N_2} = 0.12, I_o = 1.6x10^9 W/cm^2

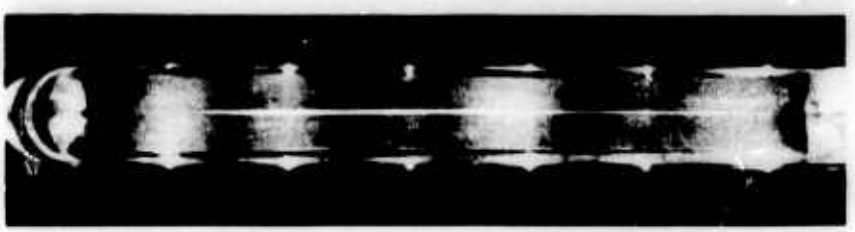

(c) p = 12.0 atm, X_{N_2} = 0.13, I_o = 1.2x10^9 W/cm^2

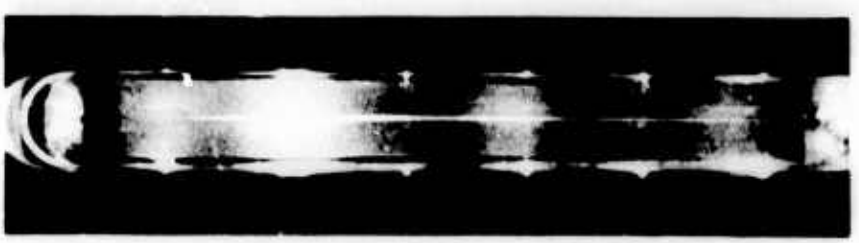

(d) p = 12.0 atm, X_{N_2} = 0.13, I_o = 1.4x10^9 W/cm^2

R09–194–2

FIG. 3.3

3371 Å PULSE SHORTENING IN He/N_2 MIXTURES

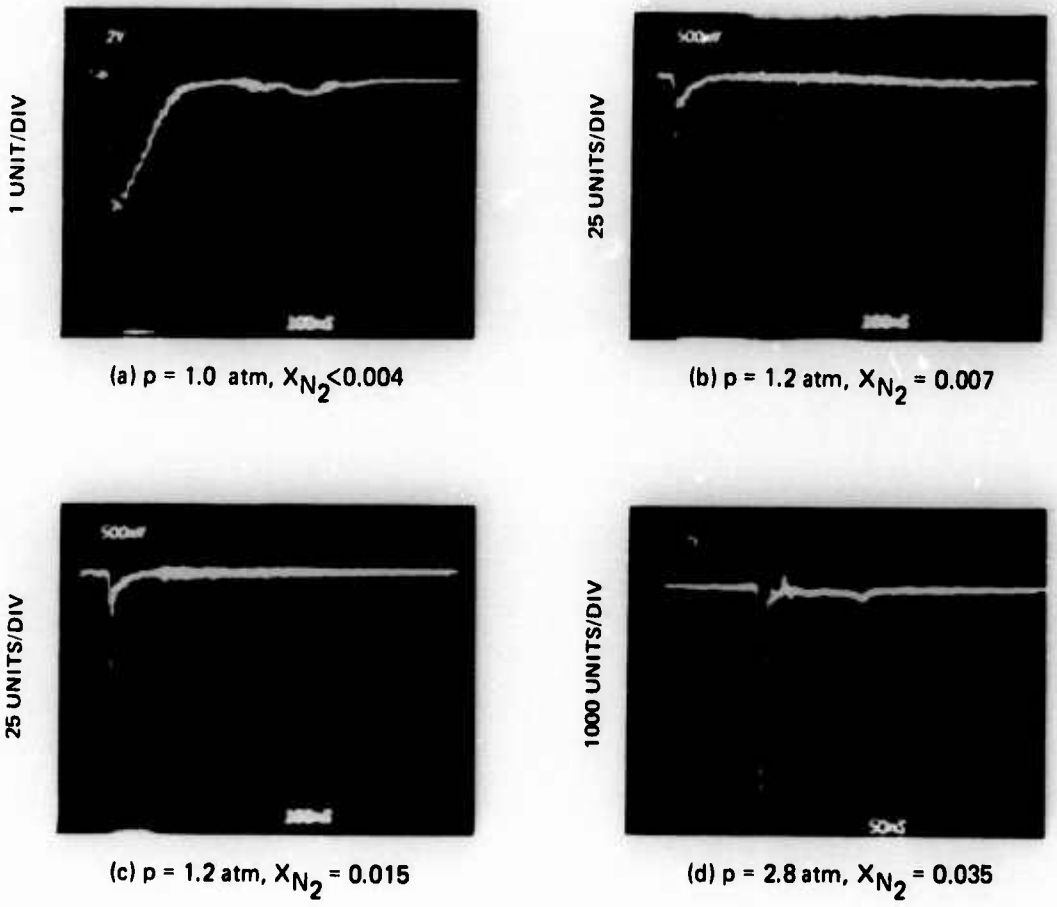

(a) p = 1.0 atm, X_{N_2}<0.004

(b) p = 1.2 atm, X_{N_2} = 0.007

(c) p = 1.2 atm, X_{N_2} = 0.015

(d) p = 2.8 atm, X_{N_2} = 0.035

R09–194–3

FIG. 3.4

COMPARISON BETWEEN MEASURED 3371 Å SIGNAL AND CALCULATED POPULATION INVERSION FOR VARIOUS 10.6μ PEAK INTENSITIES

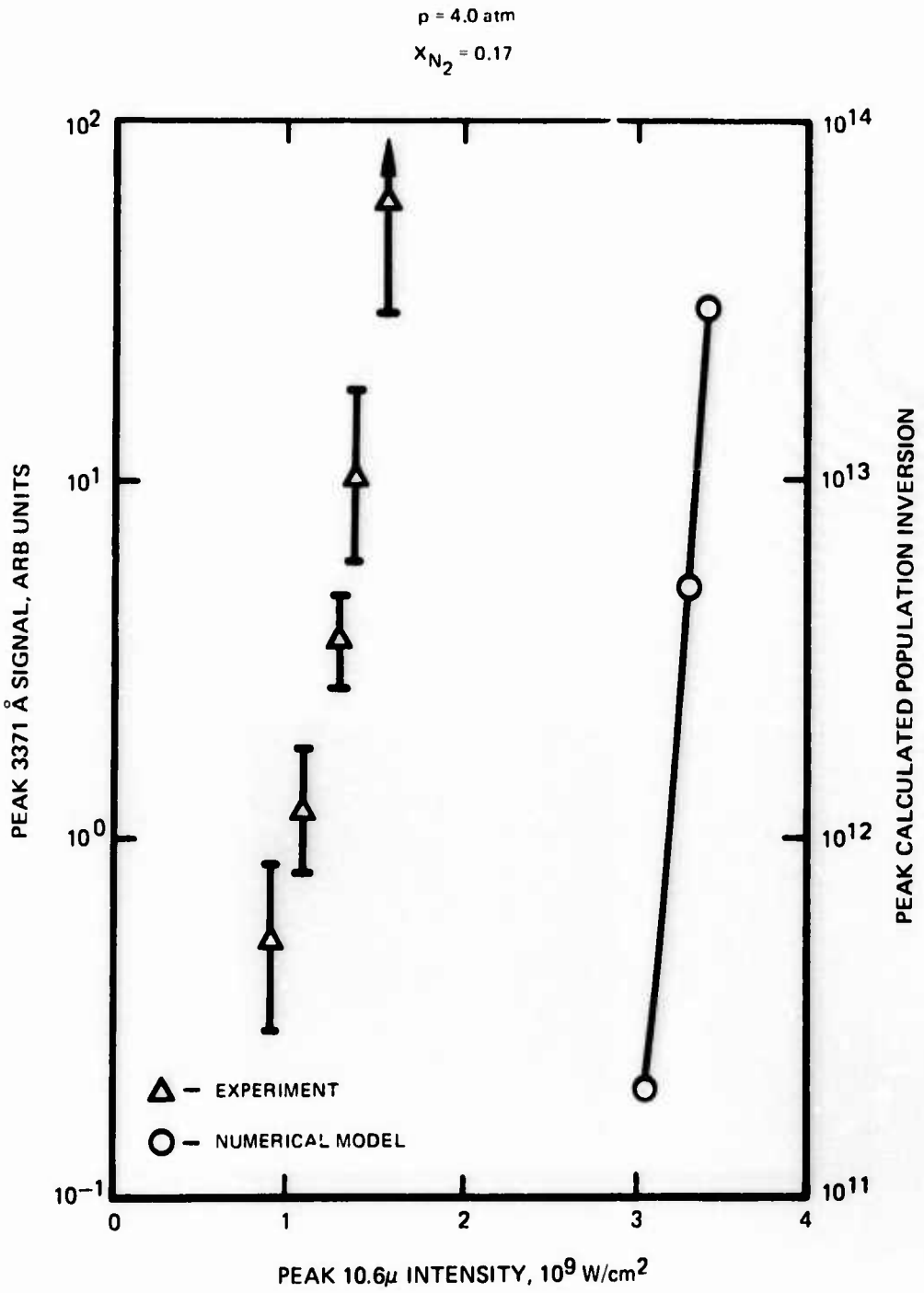

R09–194–4

RATE COEFFICIENTS USED IN THE NUMERICAL MODEL (NUMBERS CORRESPOND TO TABLE 3.1)

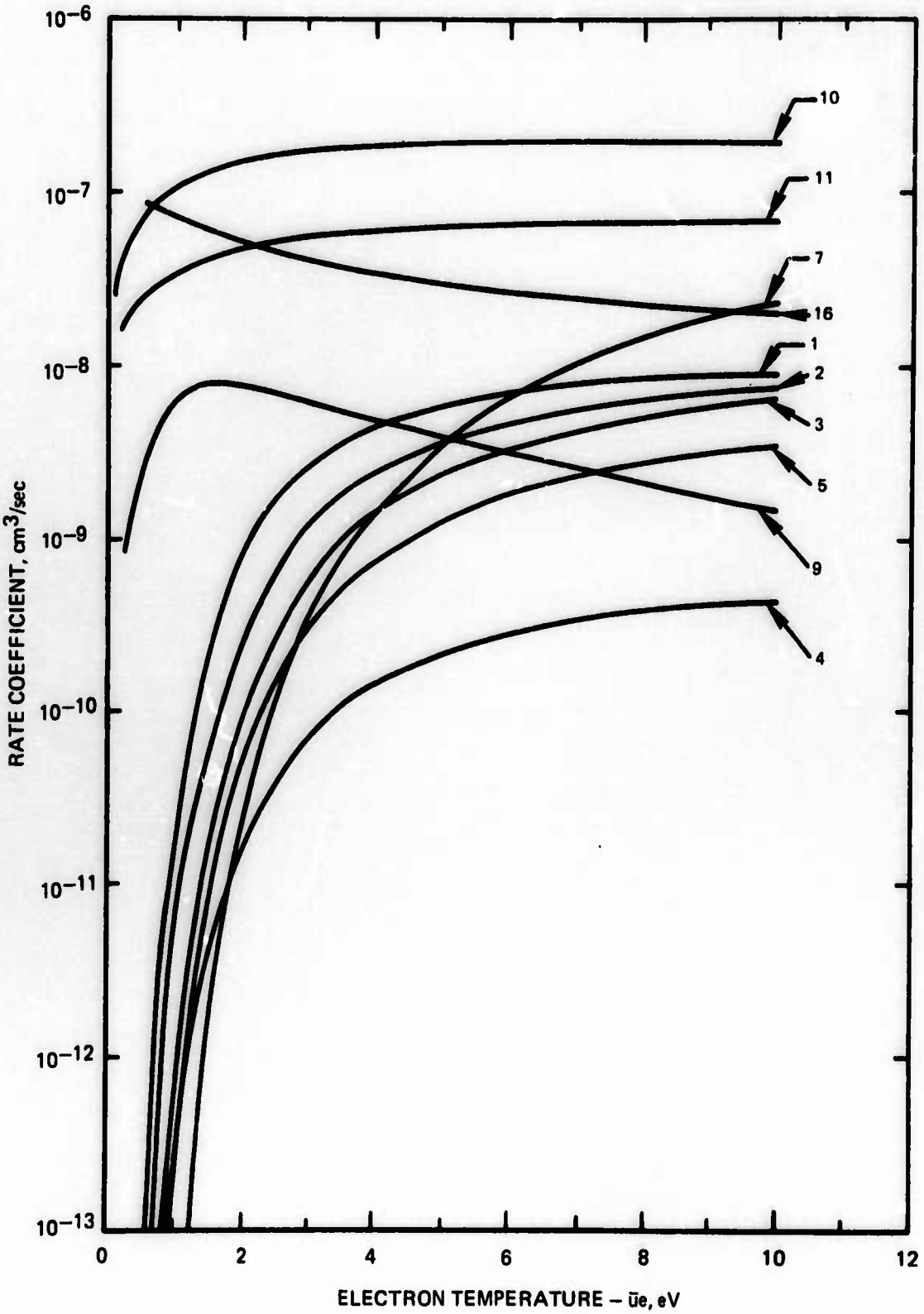

R09-194-5

FIG. 3.6

CALCULATED INVERSION DENSITIES AND ELECTRON DENSITIES FOR VARIOUS 10.6μ PEAK INTENSITIES (FOR COMPARISON, THE 10.6μ PULSE SHAPE IS SHOWN)

$p = 4.0$ atm, $X_{N_2} = 0.17$

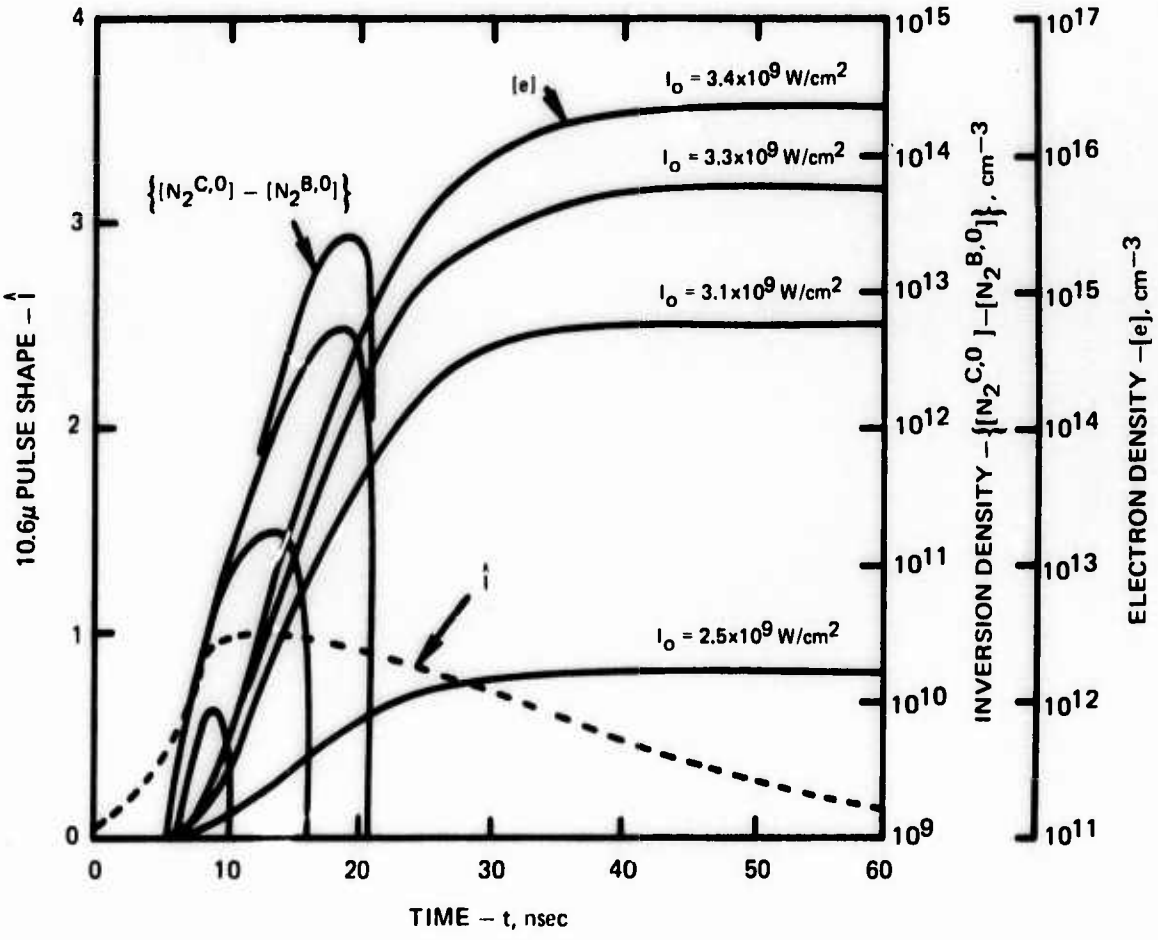

R09-194-6

FIG. 3.7

ENERGY COUPLING EFFICIENCY VS ELECTRON ENERGY

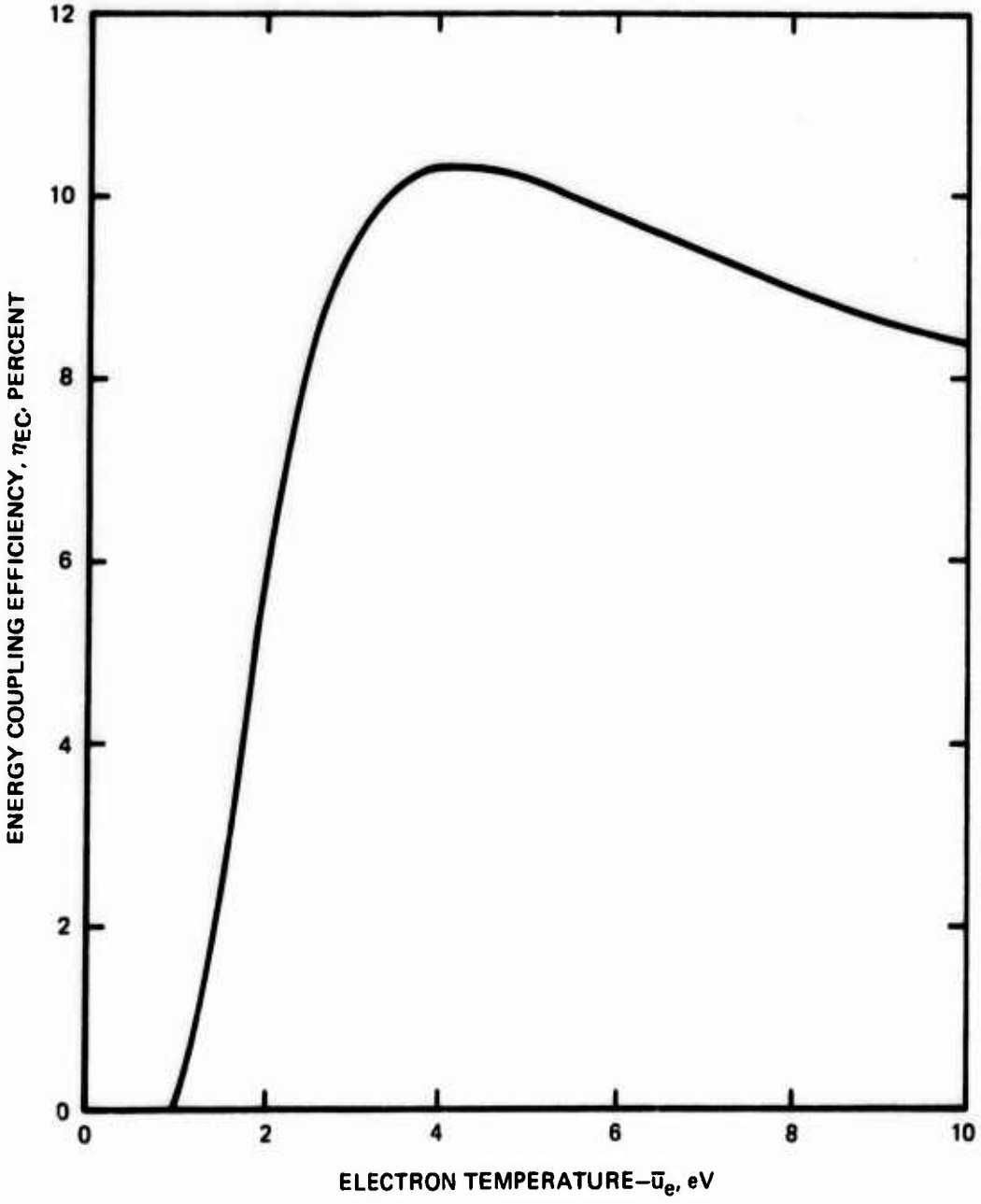

R09-194-7

FIG. 3.8

CALCULATED DISCHARGE PROPERTIES IN He/N_2 VS TIME

$p = 0.4$ atm, $X_{N_2} = 0.10$, $\ell_d = 1.0 \times 10^2$ cm

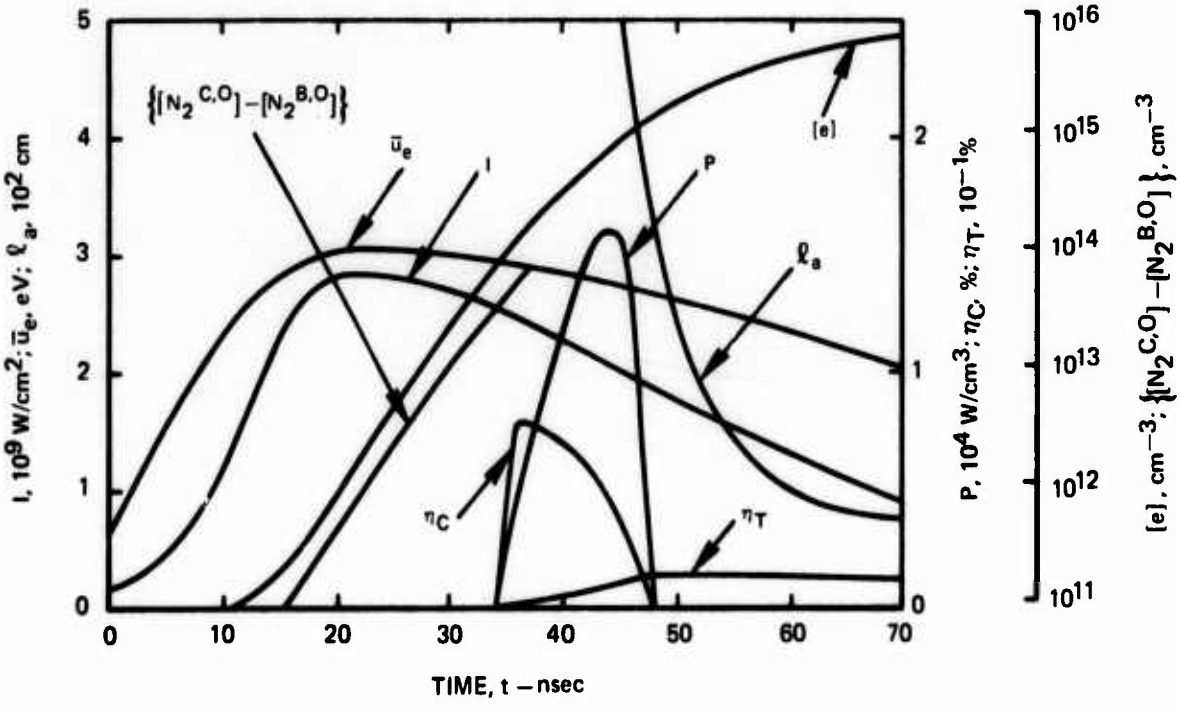

I – 10.6μ INTENSITY, $\bar{u}_e$ – ELECTRON ENERGY, ℓ_a – 10.6μ ABSORPTION LENGTH, P – uv POWER DENSITY
η_C – COUPLING EFFICIENCY, η_T – TOTAL EFFICIENCY, [e] ELECTRON DENSITY,
$\{[N_2{}^{C,O}]-[N_2{}^{B,O}]\}$ – INVERSION DENSITY

R09–194–8

CALCULATED DISCHARGE PROPERTIES IN He/N_2 VS TIME

$p = 2.0$ atm, $X_{N_2} = 0.02$, $\ell_d = 5.0 \times 10^2$ cm

THE SYMBOLS USED ARE THE SAME AS IN FIG. 8

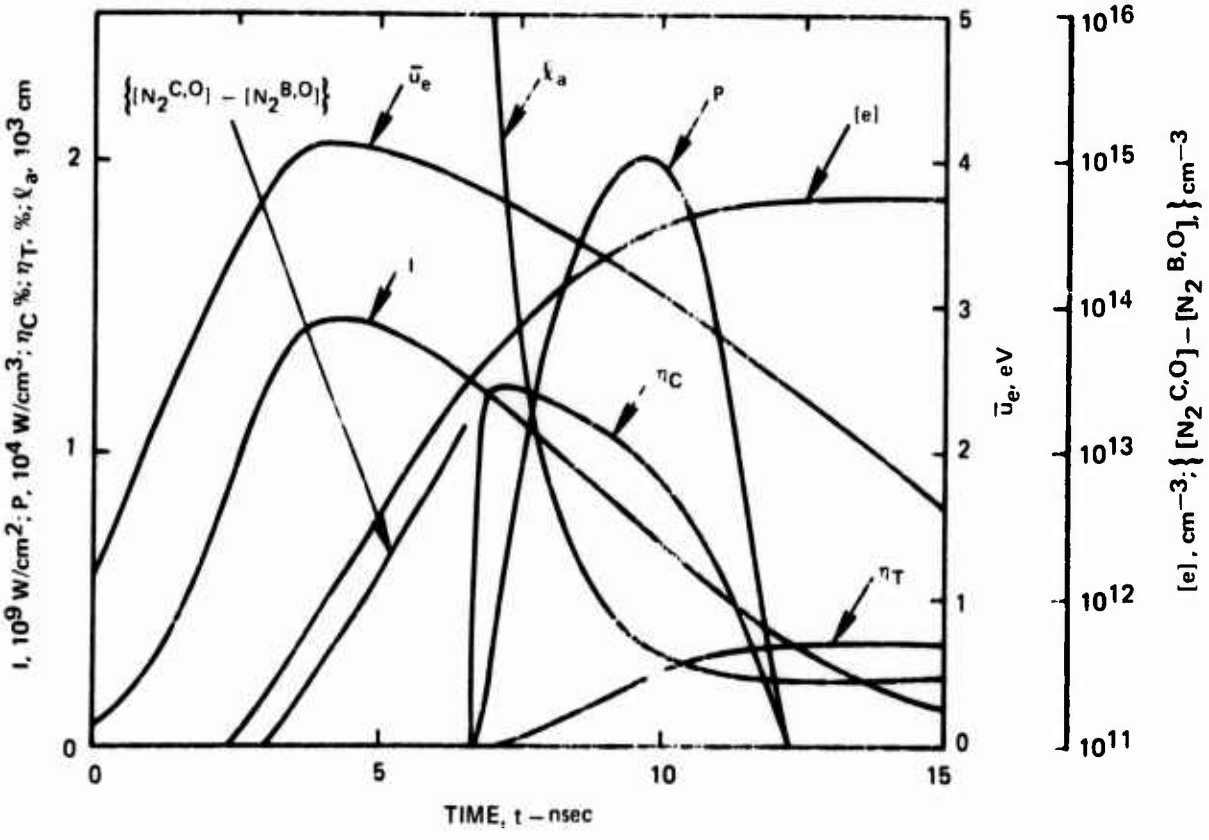

R09-194-9

14. J

FIG. 3.10

EXPERIMENTAL ARRANGEMENT USED IN COAXIAL STUDIES WITH He/N_2 AND WITH LARGE TEA LASER IN UNSTABLE RESONATOR MODE

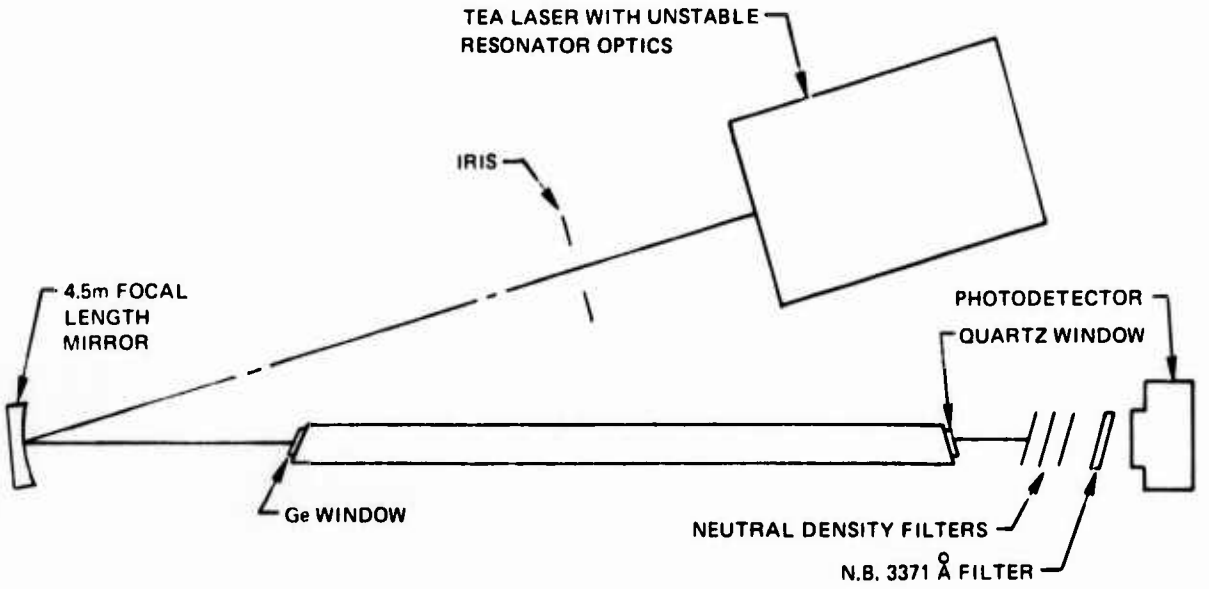

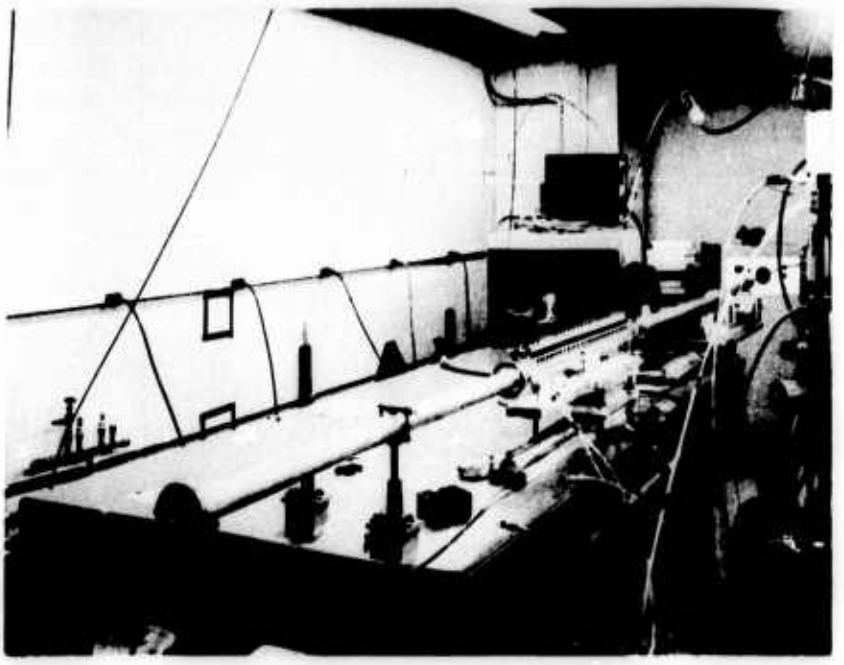

R09-194-10

M. K

10.6μ LASER UNSTABLE RESONATOR BEAM PROFILES

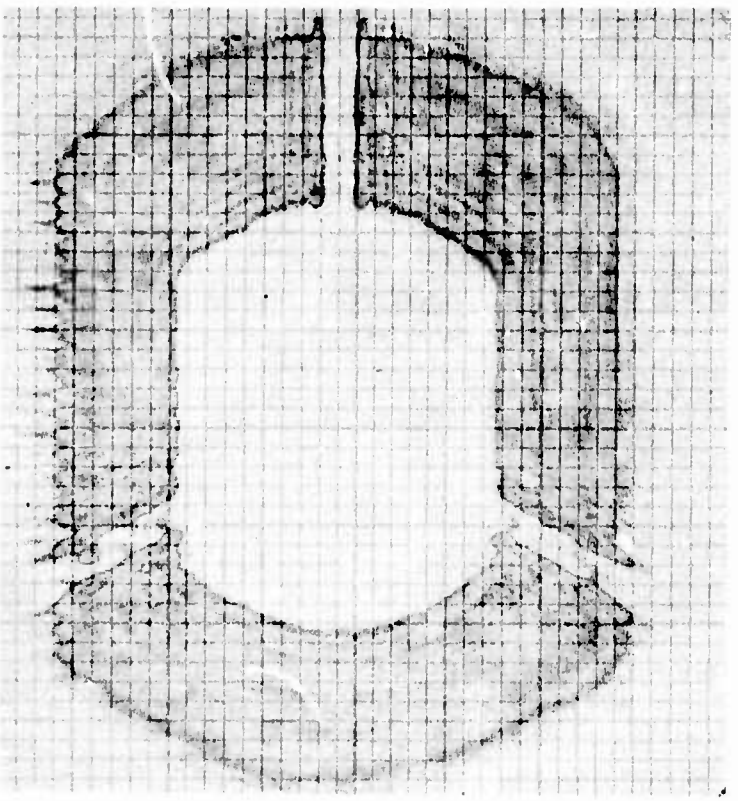

(a) BEAM AT EXIT OF LASER

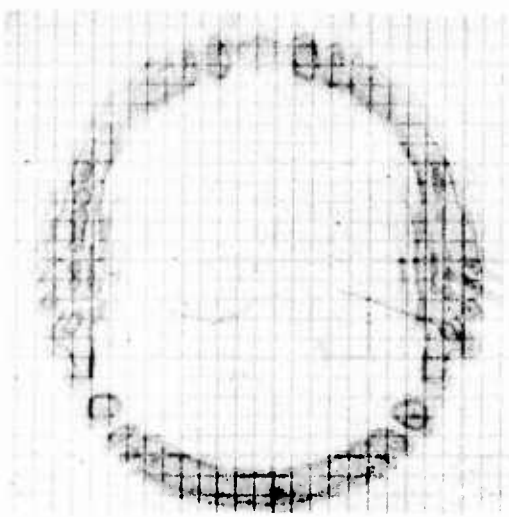

(b) BEAM AT EXIT OF APERTURE

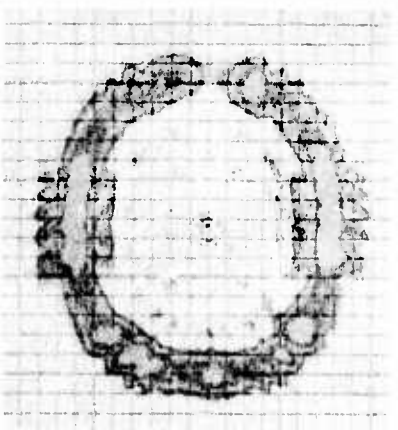

(c) BEAM AT ENTRANCE TO CELL

R09-194-11

FIG. 3.12

OPTICALLY PUMPED DISCHARGE

p = 1.0 atm, $X_{N_2} = 0.05$, $X_{He} = 0.95$

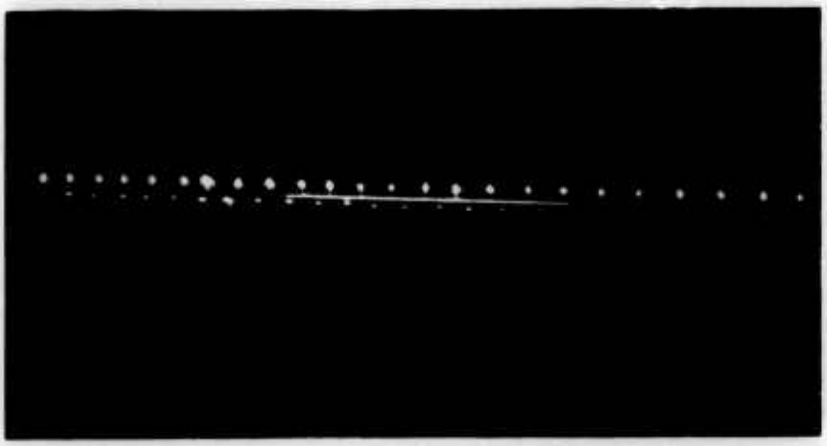

(a) 10.6μ PEAK INTENSITY JUST BELOW BREAKDOWN THRESHOLD

(b) 10.6μ PEAK INTENSITY JUST ABOVE BREAKDOWN THRESHOLD

R09–194–12

FIG. 3.13

LASER SPOT AND CORRESPONDING DETECTOR TRACE FROM OPEDL AT 3371 Å (AMPLIFIED SPONTANEOUS EMISSION MODE)

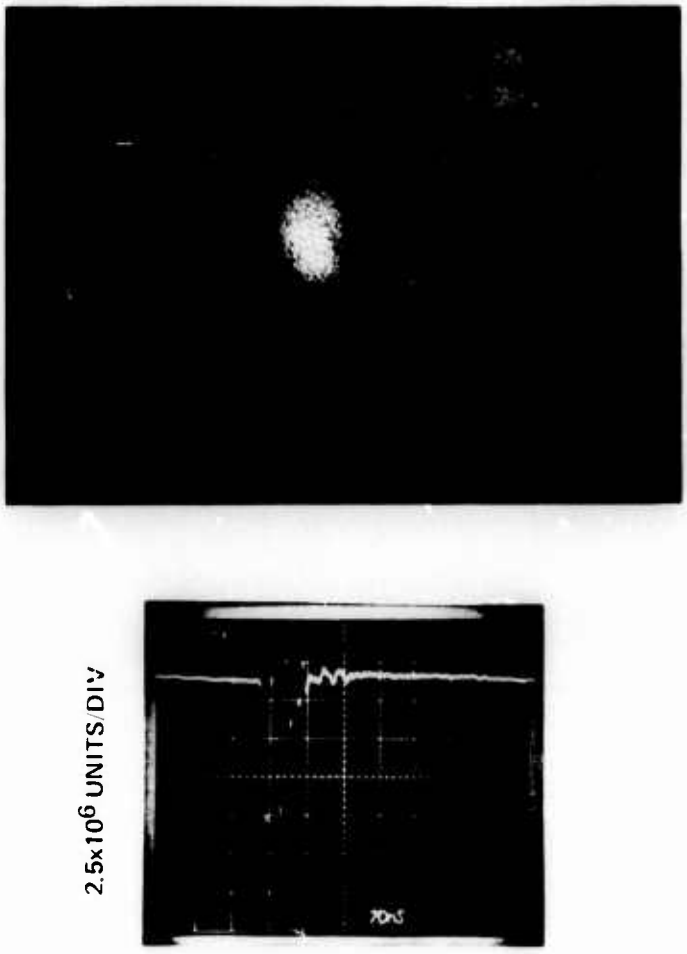

3371 Å LASER SPOTS WITH SINGLE-PASS OPTICAL CAVITY

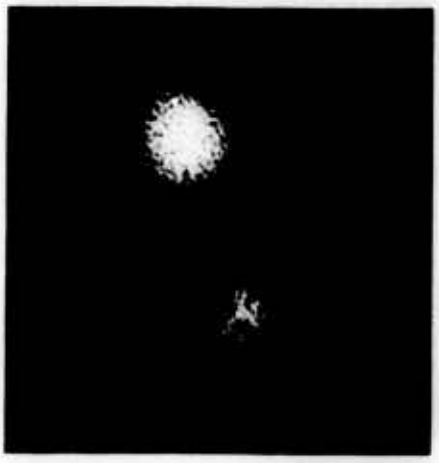

(a) uv MIRROR MIS-ALIGNED, CAMERA AT f 4.5

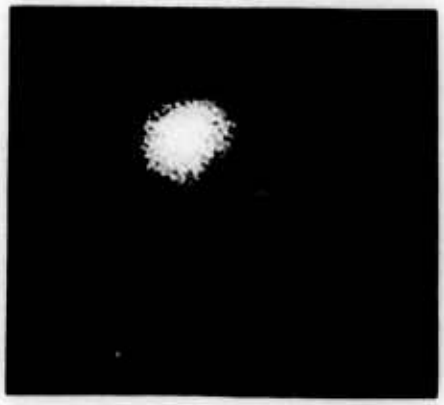

(b) uv MIRROR ALIGNED, CAMERA AT f 4.5

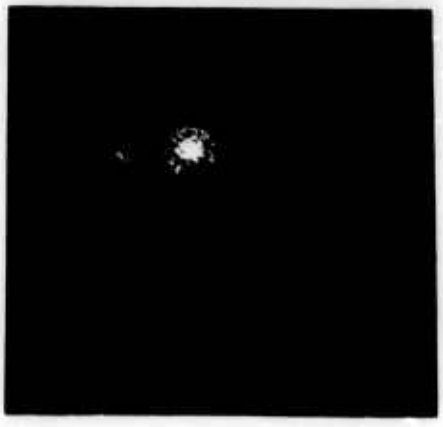

(c) uv MIRROR ALIGNED, CAMERA AT f 16

3371 Å DETECTOR TRACES WITH SINGLE – PASS OPTICAL CAVITY

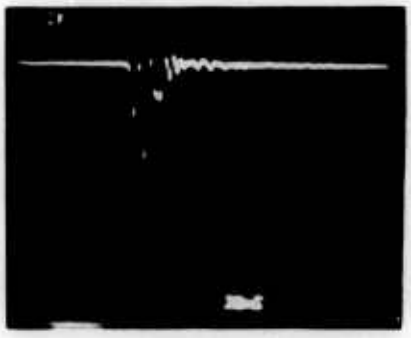

DIRECT PULSE

DIRECT PULSE

COMPOSITE PULSE

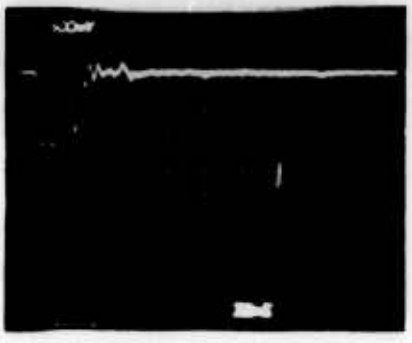

COMPOSITE PULSE

SECTION 4

STUDIES AT 3577 Å IN HELIUM/ARGON/NITROGEN MIXTURES

As discussed in Section 3 above, the He/N_2 system, using direct electron pumping of the upper laser level, appears to have inherent efficiency limitations. Therefore, studies are continuing into the applicability of the optically pumped discharge to other systems, such as the Ar/N_2 excitation transfer system (ABO74, ABB75).

4.1 Experimental Studies with Small TEA Laser

Studies were carried out with various mixtures of $He/N_2/Ar$ using the arrangement shown in Fig. 3.1. The objective of these experiments was to obtain data similar to those in Fig. 3.3, but at 3577 Å and corresponding to transfer from excited argon to the $C(3\pi_u)_{v'=0}$ state of the nitrogen. A photo of a typical discharge, along with a typical detector trace at 3577 Å are shown in Fig. 4.1. A plot of the peak uv signal for increasing values of 10.6μ intensity is shown in Fig. 4.2. While the signal does increase rapidly with increasing pumping (up to the breakdown limit), the medium does not support amplified spontaneous emission for these conditions. This result is not surprising since the small signal gain of the Ar/N_2 charge transfer system, while quite large (ABB75), is much smaller than for the direct-pumped nitrogen system. Further studies with the Ar/N_2 system will be carried out when a pumping geometry suitable for use with an optical cavity has been developed.

4.2 Theoretical Studies

A computer model similar to that for He/N_2, described in Section 3, and similar to that in Ref. (ABB75) has been developed for the $He/Ar/N_2$ system. Rate data have been taken from Ref. (HGHML74), and the $C(3\pi_u)_{v'=1}$, $B(3\pi_g)_{v'=0}$, and $B(3\pi_g)_{v'=0}$ levels have been treated separately. The uv laser radiation field has been treated in a manner similar to that in Section 3; i.e., the uv power density is assumed to be zero until the small signal gain reaches threshold, at which point the 3577 Å transition is assumed to be saturated. A typical set of calculated curves is shown in Fig. 4.3, in which a very short 10.6μ pulse was used. For this case, the threshold condition was based on an optical cavity with mirror reflectivities of 80 percent each. For these particular conditions, two uv laser pulses occurred. The first was due to direct electron pumping of the $C(3\pi_u)_{v'=0}$ level, and the second was due to transfer from excited argon.

A considerable amount of numerical experimentation was carried out with this code, and it was found that various quenching processes degrade the predicted efficiency of this system. However, the validity of the present model is subject to serious question, since it predicts bottlenecking of the lower laser level, in contrast to the quasi-cw operation recently reported in Ref. (ABB75). Attempts to determine the correct rates as well as comparisons with OPEDL data will be carried out during the next reporting period.

FIG. 4.1

DISCHARGE AND DETECTOR TRACE IN $He/Ar/N_2$

SMALL TEA LASER

$p = 4.0$ atm, $X_{N_2} = 0.17$

$X_{Ar} = 0.33$, $X_{He} = 0.50$

3577 Å

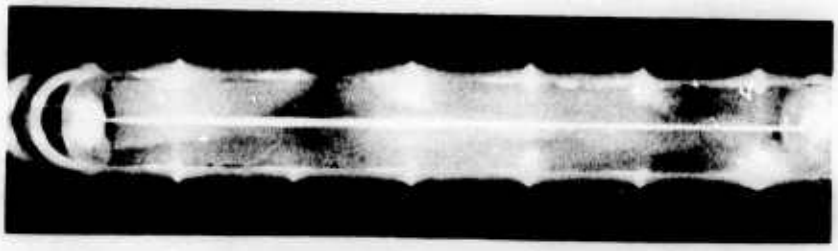

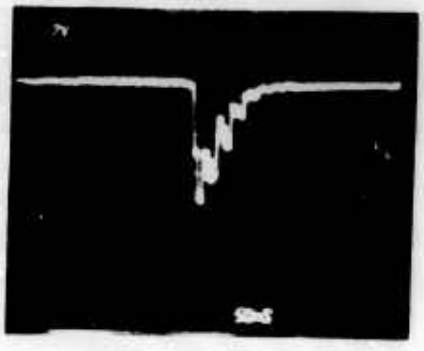

10 UNITS/DIV.

R09–194–16

K-A

FIG. 4.2

uv DETECTOR SIGNAL VS 10.6μ PUMPING INTENSITY

p = 4.0 atm X_{N_2} = 0.17 X_{Ar} = 0.33 X_{He} = 0.50

3577 Å

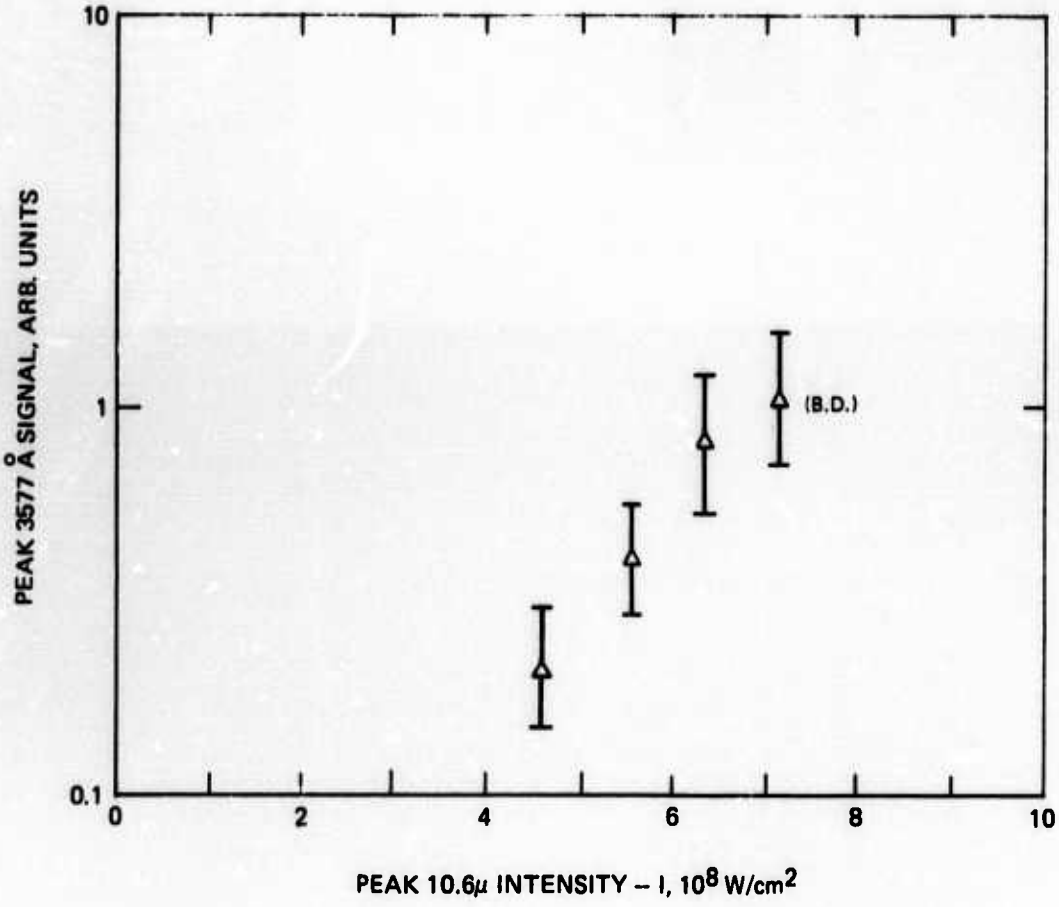

R09–194–17

FIG. 4.3

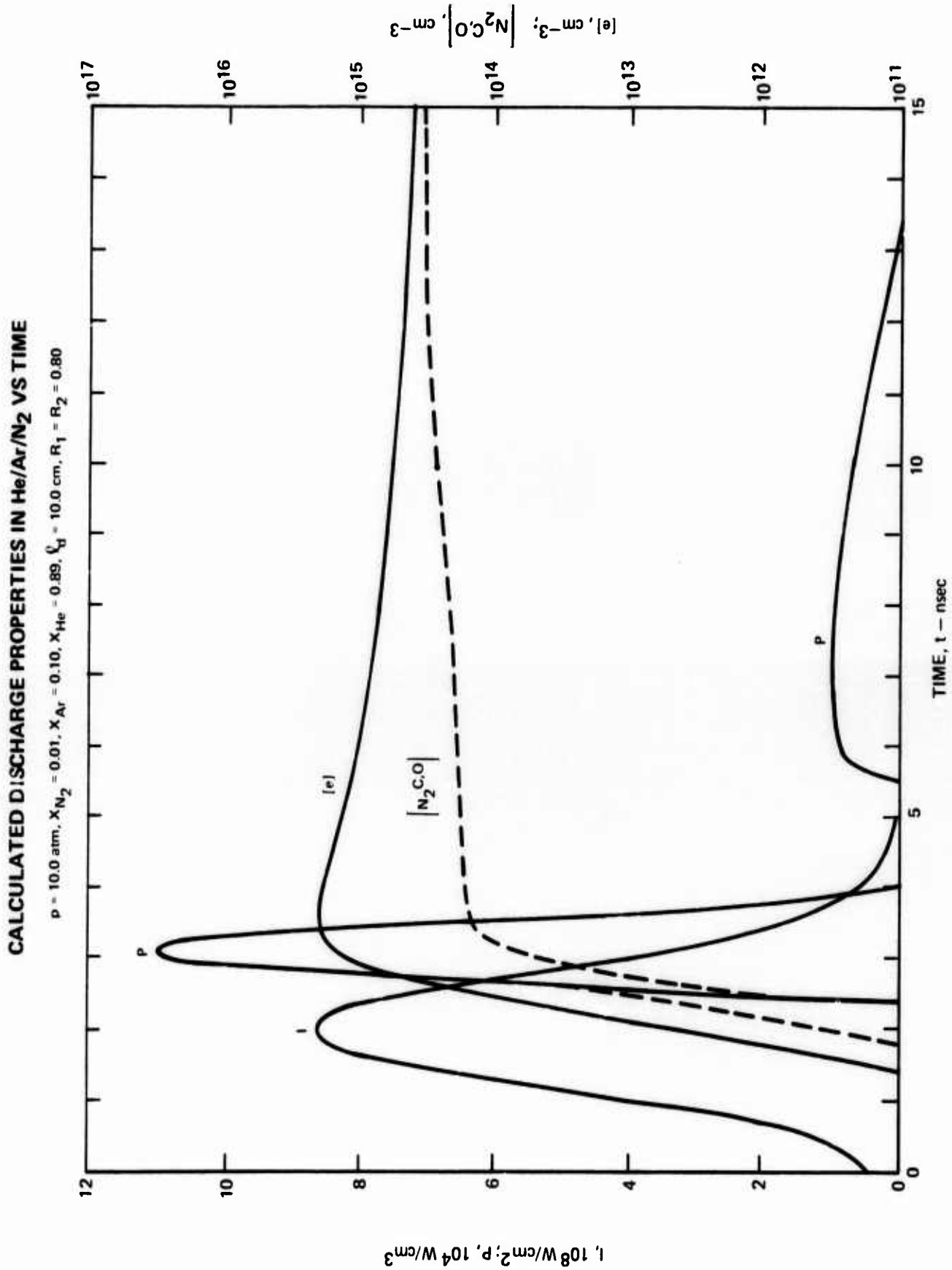

R09-194-18

SECTION 5

PUMPING CONFIGURATION STUDIES

One of the major objectives of this program is to develop optical pumping configurations which will allow the incorporation of an effective uv/visible cavity into the discharge cell. The arrangement shown in Fig. 5.1 has recently been used in conjunction with the large TEA laser, and shows considerable promise. The TEA laser was operated with a multi-mode cavity, giving a pulse with properties listed in Table 2.1. An annular beam was formed by using a large iris and a small disc mounted on a strut to block portions of the beam. The primary reason for tailoring the beam shape was to minimize extraneous 10.6μ reflections, which tended to damage the coatings on the Ge cell window. Typical beam profiles are shown in Fig. 5.2. A photo of the cell side-window, along with typical discharges obtained with the multi-mode configuration are shown in Fig. 5.3. These discharges were operated at high pressures of He, with small fractions of N_2, and correspond to good operating points for the nitrogen ion-charge transfer laser at 4278 Å (CC75). Appropriate optics for this transition will be incorporated into the cell in the near future.

The cell used in Fig. 5.3 was the same as that in Fig. 3.2, and it can be seen that the total discharge volume has been increased by over two orders of magnitude. In addition, it was discovered that a more uniform discharge was obtained using only a single spark source for the preionization. The photo in Fig. 5.3-c, in which the Polaroid film was not saturated, shows that the discharge was uniform and diffuse over a region ~1 cm in diameter by ~15 cm long. End view photographs showed that the discharge was approximately cylindrical in shape. The intense region at the left end of the discharge in Fig. 5.3-d appears to be near the breakdown threshold, and one can infer an electron density there in the 10^{15} - 10^{16} cm^{-3} range. Detailed measurements of the properties of these discharges will be made during the next reporting period.

FIG. 5.1

PUMPING CONFIGURATION UTILIZING MULTI–MODE 10.6 μ BEAM

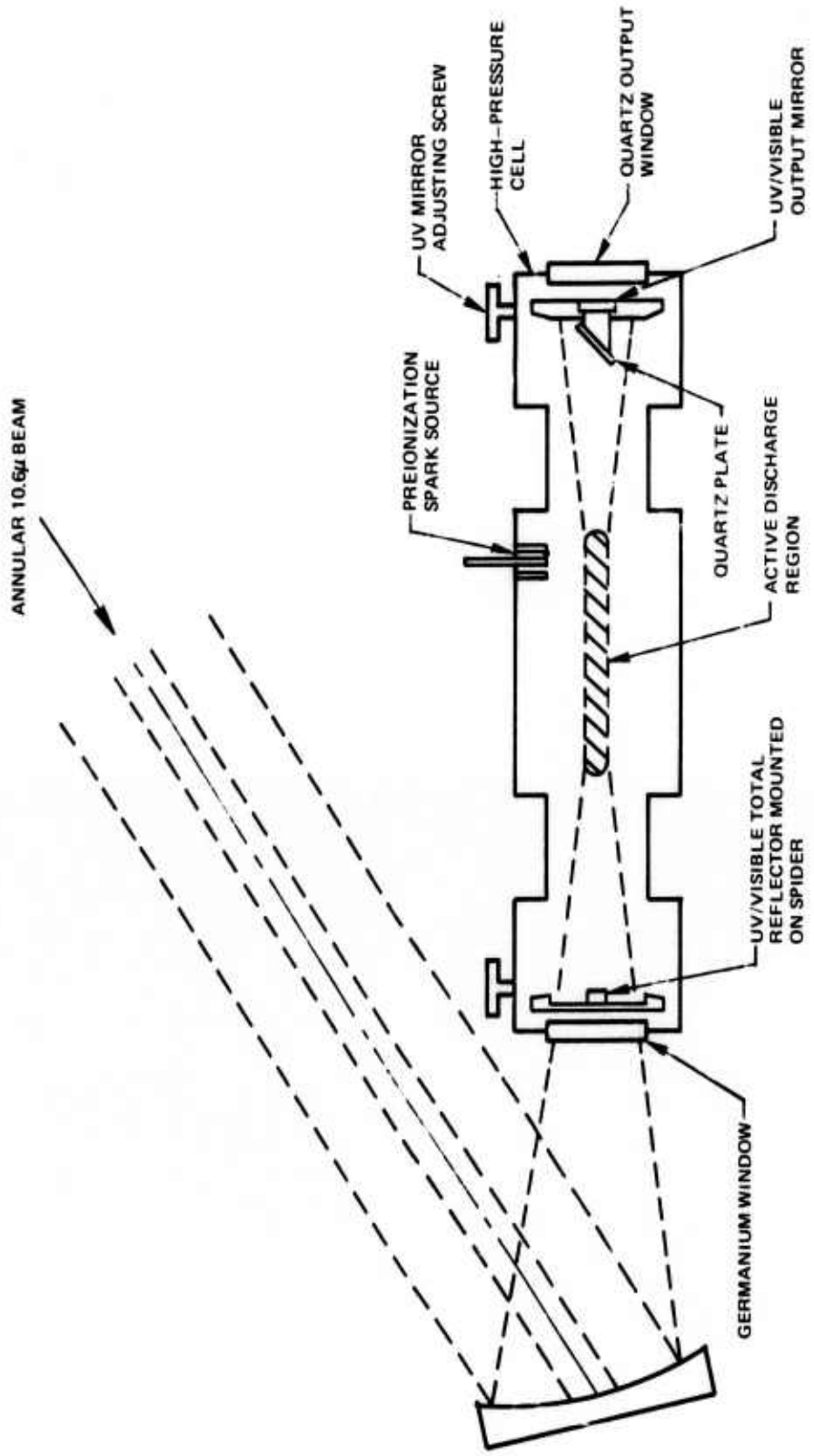

R09–194–19

MULTI-MODE BEAM PROFILES

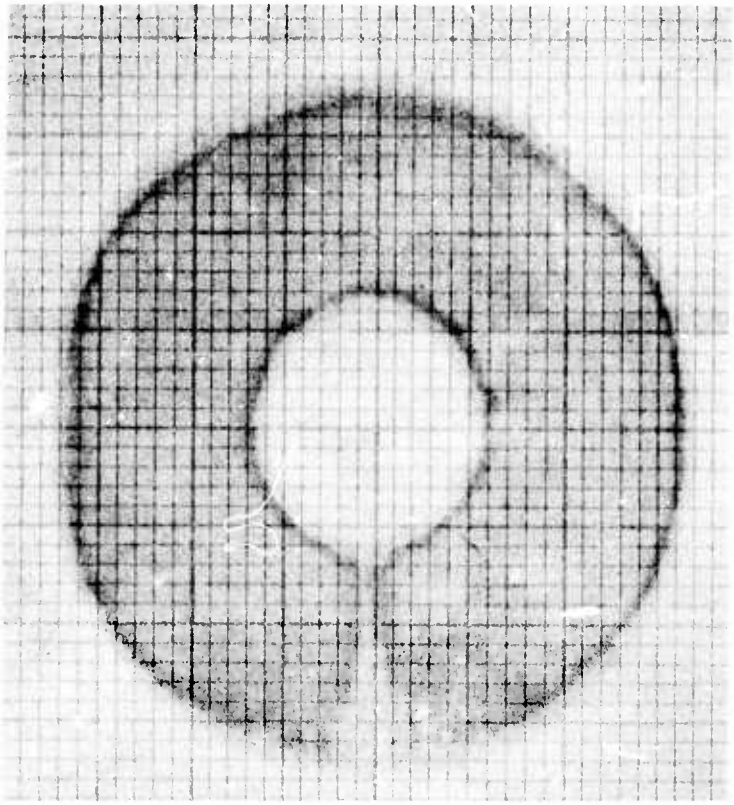

(a) BEAM AT FOCUSING MIRROR

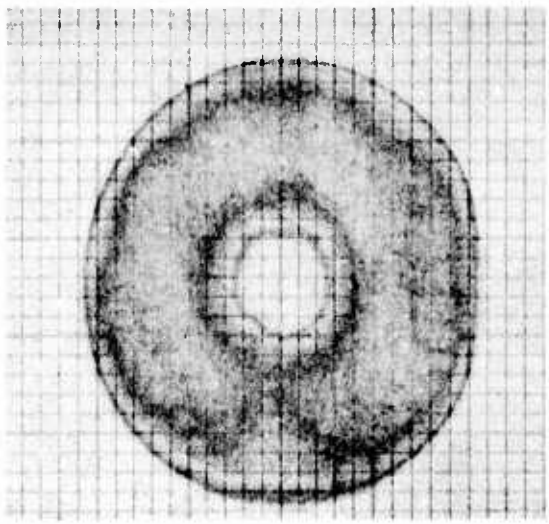

(b) BEAM AT CELL ENTRANCE WINDOW

R09-194-20

OPTICALLY PUMPED DISCHARGES WITH THE MULTI-MODE CONFIGURATION

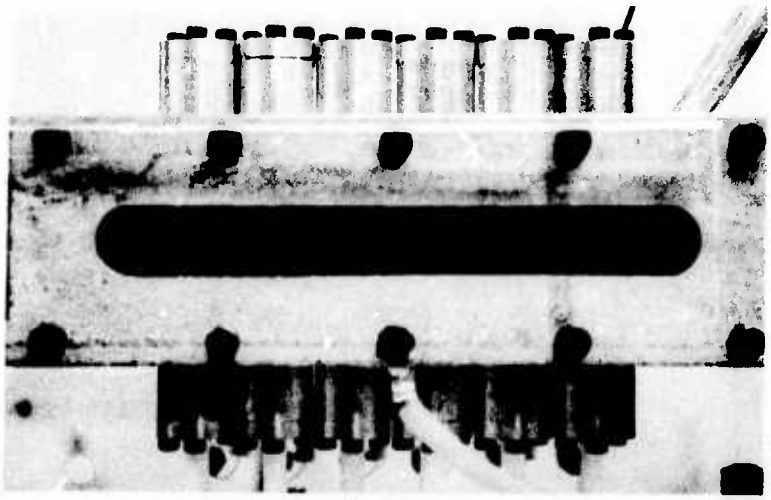

(a) CELL

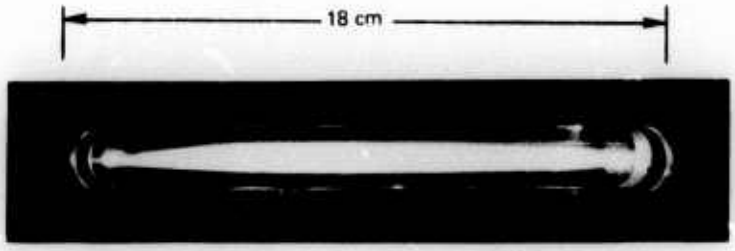

(b) p_{He} = 10.0 atm p_{N_2} = 10 torr CAMERA AT f 11

(c) p_{He} = 10.0 atm p_{N_2} = 10 torr CAMERA AT f 32

(d) p_{He} = 20.0 atm p_{N_2} = 80 torr CAMERA AT f 32

SECTION 6

FUTURE PLANS

During the next reporting period, investigations of the optically-pumped high-pressure electric discharge laser will be continued. Based on the success to date with the multi-mode coaxial configuration, initial efforts will be directed toward incorporating an optical cavity into this configuration. Studies will be made with the helium/nitrogen charge transfer system at 4278 Å and with the argon/nitrogen excitation transfer system at 3577 Å. Coaxial studies will also be carried out in some of the recently developed rare gas-halogen systems, such as KrF. In addition to the coaxial configuration, discharge studies with other optical geometries such as transverse cylindrical focusing, and the axicon geometry are planned.

Theoretical modeling studies will be continued. While many of the rates are not yet available for the newer systems, calculations will be carried out for those systems for which the appropriate rates are known, and results will be compared directly with OPEDL data wherever possible.

REFERENCES

ABB75. Ault, E. R., R. S. Bradford, Jr., and M. L. Bhaumik: Northrup report on Contract No. N00014-72-C-0456, (May 1975).

ABO74. Ault, E. R., M. L. Bhaumik, and N. T. Olson, IEEE J. Quantum Electron. QE-10, p. 624, (1974).

AKA67. Ali, A. W., A. C. Kolb, and A. D. Anderson, Appl. Optics 6, p. 2115, (1967).

Br74. Brown, R. T.: UARL Rep. N921853-2, Semi-Annual Technical Report on ARPA Contract No. N00014-74-C-0376, (Oct. 1974).

BS73. Brown, R. T., and D. C. Smith: Appl. Phys. Letters 22, p. 245, (1973).

Ca70. Cartwright, D. C., Phys. Rev. A 2, p. 1331, (1970).

CC75. Collins, C. B., and A. J. Cunningham, Appl. Phys. Letters 27, p. 127, (1975).

CCS74. Collins, C. B., A. J. Cunningham, and M. Stockton, Appl. Phys. Letters 25, p. 344, (1974).

EPR64. Engelhardt, A. G., A. V. Phelps, and C. G. Risk., Phys. Rev. A 135, p. 1566, (1964).

Ge65. Gerry, E. T., Appl. Phys. Letters 7, p. 6, (1965).

HPKB74. Hasson, V., D. Preussler, J. Klimek, and H. M. von Bergmann, Appl. Phys. Letters 25, p. 654, (1974).

HGHML74. Hill, R. M., R. A. Gutcheck, D. L. Huestis, D. Mukherjee, and D. C. Lorentz, SRI Rept. No. MP74-39, (July 31, 1974).

KFRE72. Koehler, H. A., L. H. Ferderber, D. L. Redhead, and P. J. Ebert, Appl. Phys. Letters 21, p. 198, (1972).

Le65. Leonard, D. A., Appl. Phys. Letters 7, p. 4, (1965).

Mc64. McDaniel, E. W.: Collision Phenomena in Ionized Gases. John Wiley & Sons, Inc., New York, (1964).

SB75. Smith, D. C. and R. T. Brown, J. Appl. Phys. 46, p. 1146, (1975).

Wa73. Waynant, R. W., Laser Focus 9, p. 41, (1973).